ARL-TR-9058 ● SEP 2020

DEVCOM ARMY RESEARCH LABORATORY

Spectroscopic Characterization of Low-Phonon Erbium-Doped BaF_2 Single Crystals

by Ei Ei Brown, Zackery Fleischman, Jason McKay, and Mark Dubinskii

NOTICES

Disclaimers

The findings in this report are not to be construed as an official Department of the Army position unless so designated by other authorized documents.

Citation of manufacturer's or trade names does not constitute an official endorsement or approval of the use thereof.

Destroy this report when it is no longer needed. Do not return it to the originator.

ARL-TR-9058 ● SEP 2020

Spectroscopic Characterization of Low-Phonon Erbium-Doped BaF_2 Single Crystals

Ei Ei Brown, Zackery Fleischman, and Mark Dubinskii
Sensors and Electron Devices Directorate, CCDC Army Research Laboratory

Jason McKay
General Technical Services, LLC

REPORT DOCUMENTATION PAGE

Form Approved
OMB No. 0704-0188

1. REPORT DATE *(DD-MM-YYYY)*	2. REPORT TYPE	3. DATES COVERED (From - To)
September 2020	Technical Report	1 January–31 December 2019

4. TITLE AND SUBTITLE
Spectroscopic Characterization of Low-Phonon Erbium-Doped BaF_2 Single Crystals

5a. CONTRACT NUMBER

5b. GRANT NUMBER

5c. PROGRAM ELEMENT NUMBER

6. AUTHOR(S)
Ei Ei Brown, Zackery Fleischman, Jason McKay, and Mark Dubinskii

5d. PROJECT NUMBER

5e. TASK NUMBER

5f. WORK UNIT NUMBER

7. PERFORMING ORGANIZATION NAME(S) AND ADDRESS(ES)
CCDC Army Research Laboratory
ATTN: FCDD-RLS-RL
Adelphi, MD 20783-1138

8. PERFORMING ORGANIZATION REPORT NUMBER
ARL-TR-9058

9. SPONSORING/MONITORING AGENCY NAME(S) AND ADDRESS(ES)

10. SPONSOR/MONITOR'S ACRONYM(S)

11. SPONSOR/MONITOR'S REPORT NUMBER(S)

12. DISTRIBUTION/AVAILABILITY STATEMENT
Approved for public release; distribution is unlimited.

13. SUPPLEMENTARY NOTES
ORCID ID: Brown, 0000-0002-4102-1006

14. ABSTRACT

There is substantial attention on the development of rare-earth doped solid-state laser sources for mid-infrared (mid-IR) applications. Recently, there has been renewed interest in fluorites as laser hosts due to their low phonon energies and compatibility with rare-earth dopants. Barium fluoride (BaF_2) is particularly attractive due to its low maximum phonon energy of approximately 330 cm^{-1}. In this work, Er^{3+}-doped BaF_2 single crystals were grown by a Bridgman technique. Following optical pumping at 800 nm, Er^{3+}:BaF_2 exhibited several broad mid-IR emission bands centered at approximately 2750, 3500, and 4480 nm, corresponding to the $^4I_{11/2} \rightarrow {}^4I_{13/2}$, $^4F_{9/2} \rightarrow {}^4I_{11/2}$, and $^4I_{9/2} \rightarrow {}^4I_{11/2}$ transition, respectively. The multiphonon decay rates of several closely spaced Er^{3+} transitions were modeled using the well-known energy-gap law, and the host-dependent parameters B and b were determined to be 6.3×10^8 s^{-1} and 5.23×10^{-3} cm, respectively. The obtained energy-gap law parameters were subsequently used to describe the temperature dependence of the 4480-nm mid-IR emission lifetime for a range of 77 K to room temperature.

15. SUBJECT TERMS
rare-earth doped, mid-infrared, solid-state laser, erbium, fluorides

16. SECURITY CLASSIFICATION OF:			17. LIMITATION OF ABSTRACT	18. NUMBER OF PAGES	19a. NAME OF RESPONSIBLE PERSON
a. REPORT	b. ABSTRACT	c. THIS PAGE			Ei Ei Brown
Unclassified	Unclassified	Unclassified	UU	19	19b. TELEPHONE NUMBER (Include area code) (301) 394-2293

Contents

List of Figures

List of Tables

1. Introduction

Thus far, lasers that operate at wavelengths in the mid-IR spectral region (3–5 μm) are of great interest for military, remote sensing, and medical applications. Progress on the development of mid-IR solid-state lasers beyond 3 μm has been limited by the lack of suitable gain materials. The challenge in achieving efficient mid-IR laser generation is the prevalence of multiphonon quenching of the mid-IR emission. Trivalent rare-earth (RE) dopants exhibit broadband transitions in mid-IR bands of interest but require hosts with low maximum phonon energies to mitigate the impact of nonradiative decay on upper laser level lifetime.[1–5] Fluorites (CaF_2, SrF_2, and BaF_2) are laser hosts of interest due to their low phonon energies, high thermal conductivities, and compatibility with RE dopants.[6–8] Trivalent erbium (Er^{3+}) is a laser active ion that can produce distinct near- and mid-IR emission lines and can be directly pumped with commercial laser diodes. Studies of visible luminescence and Judd–Ofelt modeling of Er^{3+}-doped BaF_2 crystals were reported by Bitam et al.[6] More recently, the enhancement of 3.9-μm emission from Ho^{3+} through sensitization by added Tm^{3+} dopant has been reported in BaF_2 via approximately 800-nm excitation.[9] Many studies on the RE-doped fluorites (CaF_2, SrF_2, CdF_2) have been reported up to the 3-μm spectral region and laser operation at 2.7 μm has been demonstrated.[7,8] Orlovskii et al. reported the multiphonon relaxation rates for the mid-IR spectral range in fluorite-type crystals doped with RE ions.[4] In this work, mid-IR (3–5 μm) emission characteristics are explored for Er^{3+}-doped BaF_2 single crystals, which have a reported maximum phonon energy of approximately 320 cm^{-1}.[6]

2. Experimental Details

Er^{3+}-doped BaF_2 crystals were grown by traditional Bridgman technique. BaF_2 is a cubic crystal with a transparency range from 0.2 to 14 μm. The Er^{3+} concentrations in the samples were determined using inductively coupled plasma optical emission spectroscopy (ICP-OES) by Galbraith Laboratories. The room temperature absorption spectra were recorded using a Cary 6000i UV-Vis-NIR spectrophotometer and a Nicolet 6700 Fourier-transform infrared spectrometer. All mid-IR fluorescence spectra were excited by a continuous-wave Spectra-Physics Tsunami Ti:Sapphire laser (800–905 nm). Either a Horiba Fluorolog-3 system with an iHR-320 monochromator (λ_{blaze}: 2 μm, 300 grooves/mm) or a Princeton Instruments Acton SpectraPro 0.15-m monochromator (λ_{blaze}: 4 μm, 150 grooves/mm) was used to collect the mid-IR emissions. The emission signal was recorded by an Infrared Associates liquid-nitrogen-cooled InSb detector in

conjunction with a Stanford Research Systems SR830 dual-phase lock-in amplifier. Fluorescence decay measurements were carried out using the output of a pulsed (10-ns pulses, 10 Hz) Nd:YAG pumped Optical Parametric Oscillator system. The decay signal was recorded with a homemade LabVIEW program using National Instruments data acquisition system. For temperature-dependent emission studies down to 77 K, the sample was mounted on the cold finger of a two-stage closed-cycle helium refrigerator.

3. Results and Discussion

Figure 1 shows the ground state absorption cross section spectrum of Er^{3+}:BaF_2 in the 400- to 1700-nm region. The absorption cross section was calculated using an Er^{3+} concentration of approximately 1.55×10^{20} cm^{-3} for Er^{3+}:BaF_2 crystal as measured by Galbraith Laboratories Inc. using ICP-OES. The characteristic absorption bands of Er^{3+} ions were centered at approximately 1519, 977, 802, 652, 541, 486, and 406 nm. The Er^{3+} absorption band at approximately 800 nm ($^4I_{15/2}$ → $^4I_{9/2}$), which is of great importance for laser diode pumping, shows a peak absorption cross section of approximately 0.145×10^{-20} cm^2.

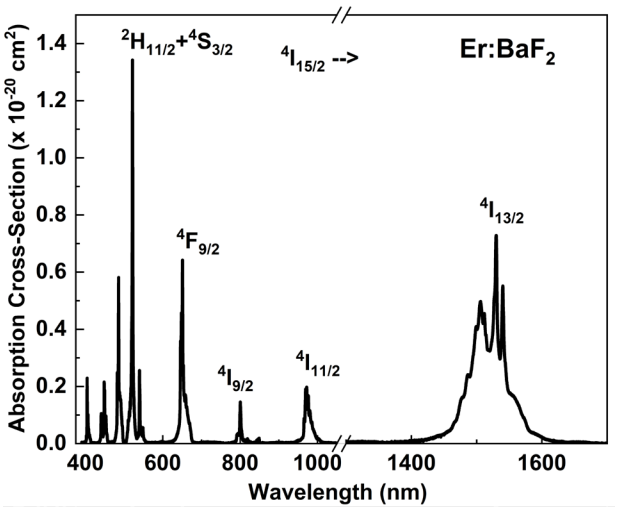

Fig. 1 Room temperature absorption cross-section spectrum of Er^{3+}:BaF_2 in the 400- to 1700-nm spectral region. Intra-4f absorption bands from the $^4I_{15/2}$ ground state to higher excited states of Er^{3+} are indicated.

Figure 2a depicts the room temperature mid-IR emission bands of Er^{3+}:BaF_2 in the wavelength ranges 2400–3100 nm, 3200–4000 nm, and 4000–5200 nm, which correspond to the $^4I_{11/2}$ → $^4I_{13/2}$, $^4F_{9/2}$ → $^4I_{9/2}$, and $^4I_{9/2}$ → $^4I_{11/2}$ transitions, respectively. Excitation of these transition upper levels was achieved using approximately 800-nm pumping, which directly populated the $^4I_{9/2}$ level and

subsequently the $^4I_{11/2}$ level through radiative and nonradiative transitions, while the $^4F_{9/2}$ level was populated through an upconversion process. Broad mid-IR emissions centered at approximately 4.48, 3.5, and 2.74 μm, consisting of weakly structured Stark components, were observed with bandwidths of approximately 0.325, 0.280, and 0.095 μm at full width at half maximum, respectively. Soulard et al. studied spectroscopic properties of 3.5-μm emission from Er-doped fluoride crystals and reported related laser operating parameters.[10] A schematic diagram of the relevant lower-lying Er^{3+} levels indicating the pump transition and observed emission lines are also illustrated in Fig. 2b.

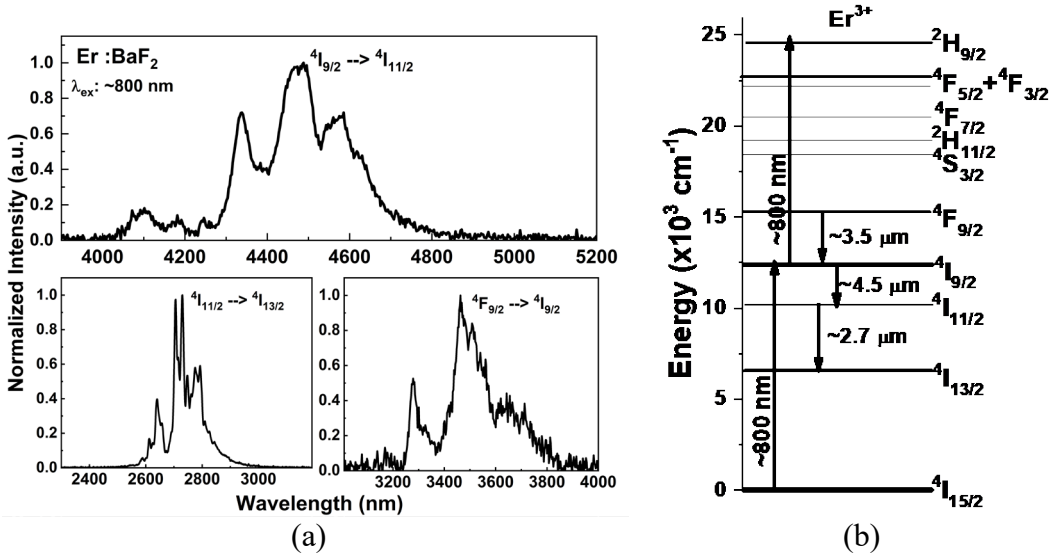

Fig. 2 a) Room temperature normalized IR emission spectra of $^4I_{9/2}$ → $^4I_{11/2}$, $^4I_{11/2}$ → $^4I_{13/2}$, and $^4F_{9/2}$ → $^4I_{9/2}$ transitions in Er^{3+}:BaF_2. b) The partial energy level diagram of Er^{3+} ions indicating the pump wavelength and corresponding emission transitions.

The fluorescence lifetimes of the first four excited states of Er^{3+}:BaF_2 were determined to be approximately 16 ms ($^4I_{13/2}$), 9.4 ms ($^4I_{11/2}$), 0.047 ms ($^4I_{9/2}$), and 0.396 ms ($^4F_{9/2}$). These are relatively longer lifetimes than observed in other Er-doped fluorides,[10–13] indicating that the lower phonon energy of BaF_2 leads to reduced nonradiative relaxation (Table 1).

Table 1 Comparison of measured (experimental) lifetime values of the first four excited states for several Er-doped fluorides

Er^{3+} Energy levels	ΔE (cm^{-1})	Er:BaF_2 (ħω~330 cm^{-1}) τ_{expt}	Er:$LiYF_4$ (ħω~490 cm^{-1}) τ_{expt} [11]	Er:KY_3F_{10} (ħω~420 cm^{-1}) τ_{expt} [12]	Er:CaF_2 (ħω~495 cm^{-1}) τ_{expt} [10–13]
$^4I_{13/2}$	6586	16 ms	13.6 ms	9.9 ms	9 ms
$^4I_{11/2}$	3650	9.4 ms	4.6 ms	5.6 ms	5.6 ms
$^4I_{9/2}$	2200	47 µs	7 µs	5 µs	6.6 µs
$^4F_{9/2}$	2881	396 µs	80 µs	228 µs	160 µs

The 4.48-µm emission properties of Er:BaF_2 were further explored to evaluate the mid-IR laser potential. Temperature-dependent emission lifetimes of $^4I_{9/2}$ level were carried out for Er^{3+}:BaF_2 over a temperature range from 77 to 300 K. Under approximately 800-nm ($^4I_{15/2}$ → $^4I_{9/2}$) excitation, the emission lifetimes monitored at approximately 1760 nm ($^4I_{9/2}$ → $^4I_{13/2}$) were determined to be approximately 0.047 and 0.13 ms at 300 and 77 K, respectively (Fig. 3a). The temperature dependence of the $^4I_{9/2}$ lifetime reflects the strong emission quenching by approximately 64% between 77 and 300 K (Fig. 3b). Judd–Ofelt analysis[6] yielded a radiative lifetime of 10.45 ms for the $^4I_{9/2}$ state, which suggests a quantum efficiency of less than 1% at room temperature. Such a low efficiency could be attributed to nonradiative decay processes such as multiphonon relaxations, energy transfer between RE ions, or energy transfer to other impurities in the crystal.

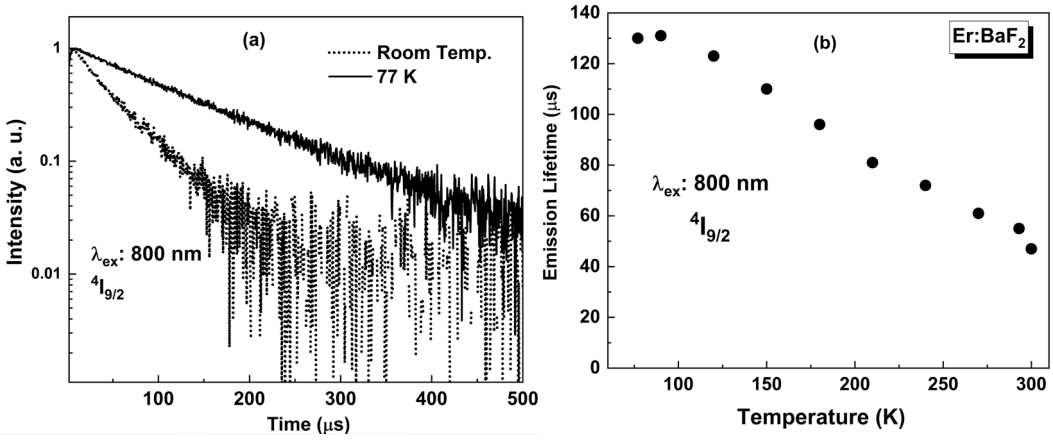

Fig. 3 a) Decay transients of Er:BaF_2 monitored at approximately 1760 nm ($^4I_{9/2}$ → $^4I_{13/2}$) for 77 K and room temperature. b) Temperature dependence of the $^4I_{9/2}$ level lifetime values between 77 K and room temperature.

The possibility of multiphonon relaxations as the cause for the observed $^4I_{9/2}$ state emission quenching in Er^{3+}:BaF_2 was further investigated. The exponential energy-gap law, which describes the rate of nonradiative decay (W_{nr}) through multiphonon relaxation processes, can be expressed as[14]

$$W_{nr} = Be^{-\beta\Delta E}\left[1 - e^{-\left(\frac{\hbar\omega}{kT}\right)}\right]^{-p} \quad (1)$$

where ΔE is the energy to the next lower level, T is the temperature, $\hbar\omega$ is the maximum phonon energy, p is the number of phonons needed to bridge the energy gap, and B and β are host-dependent fitting parameters. To determine the B and β parameters for Er^{3+}:BaF_2, several Er^{3+} transitions with energy gaps from 2200 to 3700 cm^{-1} were investigated for their multiphonon decay rates. The experimental and radiative lifetimes of the selected excited states as well as the corresponding energy gaps (ΔE) to the next lower states are described in Table 2. The W_{nr} rates for the selected excited states were then calculated using the following relation:

$$W_{nr} = \frac{1}{\tau_{meas}} - \frac{1}{\tau_{rad}} \quad (2)$$

where τ_{rad} is the radiative lifetime as predicted by Judd–Ofelt theory.[6] The acquired W_{nr} rates and corresponding energy gaps are shown in Fig. 4a. Fitting the measured nonradiative decay rates to the energy-gap law, Eq. 1 yielded B = 6.3×10^8 s^{-1} and β = 5.23×10^{-3} cm.

Table 2 The measured and radiative lifetimes as well as the W_{nr} rates of the selected excited states for Er^{3+}:BaF_2

ΔE (cm^{-1})	Energy level	τ_{meas} (ms)	τ_{rad} (ms)	W_{nr} ($\times 10^3$ s^{-1})
2205	$^4I_{9/2}$	0.047	10.45	21.181
2857	$^4F_{9/2}$	0.396	1.17	1.671
3155	$^4S_{3/2}$	0.56	0.797	0.531
3690	$^4I_{11/2}$	8.83	10.7	0.020

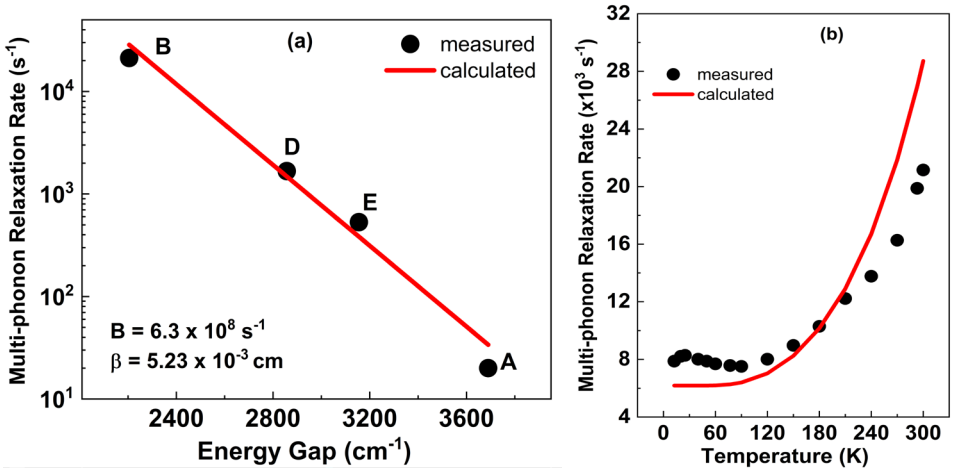

Fig. 4 a) Multiphonon decay rate (W_{nr}) as a function of energy gap (ΔE) for several Er^{3+} transitions in BaF_2. The solid line represents the best fit of the data points to the energy-gap law. b) Modeling of the nonradiative decay rate of the $^4I_{9/2}$ level using the energy-gap parameters obtained in Fig. 4a.

The obtained B and β parameters were then used to describe the temperature dependence of the measured W_{nr} rates of the $^4I_{9/2}$ level (Fig. 4b). It can be seen that some contribution of multiphonon relaxation is present in the observed decay time for Er^{3+}:BaF_2. The slight difference in the experimental lifetimes and modeled temperature dependence of the decay times suggests the existence of other nonradiative decay channels besides multiphonon relaxation, which are most likely related to energy transfer processes involving impurities or defects in BaF_2 host material. More detailed studies of the energy transfer processes are in progress.

The emission cross section of the $^4I_{9/2} \rightarrow {}^4I_{11/2}$ mid-IR transition (~4.48 μm) was calculated using the Füchtbauer–Ladenburg equation[15]:

$$\sigma_{emiss}(\lambda) = \frac{\beta\lambda^5 I(\lambda)}{8\pi n^2 c\,\tau_{rad} \int \lambda I(\lambda) d\lambda} \qquad (3)$$

where β and τ_{rad} are the branching ratio of the 4.48-μm emission ($\beta = 0.016$) and the radiative lifetime, respectively. $I(\lambda)$ is the emission intensity at wavelength λ and n is the refractive index of the host (n = 1.47). The emission cross-section spectrum for Er^{3+}:BaF_2 is depicted in Fig. 5, and its peak emission cross section at 4.48 μm was determined to be approximately 0.14×10^{-20} cm^2, which is comparable to the 4.5-μm laser transition in Er^{3+}-doped KPb_2Cl_5 (~0.17×10^{-20} cm^2).[3]

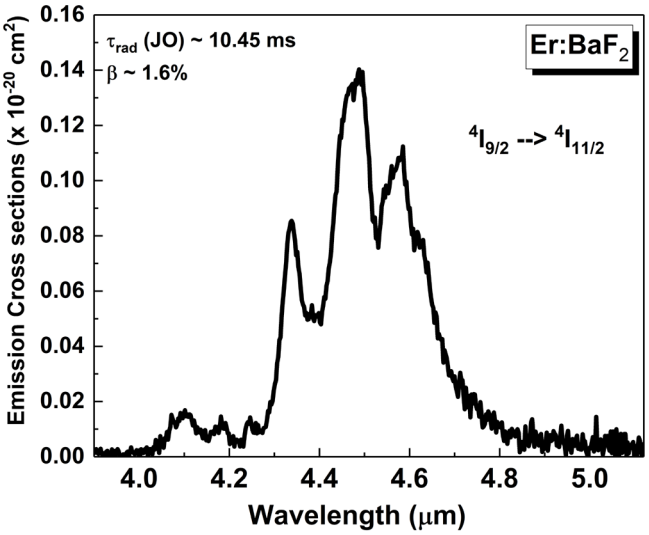

Fig. 5 Emission cross-section spectrum for the $^4I_{9/2}$ → $^4I_{11/2}$ transition in Er^{3+}:BaF_2 at room temperature

We have also investigated Er^{3+}:BaF_2 crystals co-doped with various concentrations of non-optically active ions. Studies have indicated that REs such as Er^{3+} can occupy a variety of sites in CaF_2, with significant clustering present even at dopant concentration values of less than 1%.[7,13] At higher concentration values, the clustering can lead to significant ion–ion energy transfer and higher rates of nonradiative relaxation that reduce emission efficiency. A proven technique to mitigate clustering is to co-dope the crystals with nonoptically active RE buffer ions that keep the optically active RE ions separated, which greatly reduces the ion–ion energy transfer rates. To investigate the effect of clustering on emission efficiency in Er^{3+}:BaF_2, samples were obtained with different Er^{3+} concentrations and with either charge compensating (e.g., Na^+) or RE buffer co-dopants (e.g., Gd^{3+}). The list of investigated sample matrixes is illustrated in Table 3. If clustering in Er^{3+}:BaF_2 produces significant nonradiative relaxation, one would expect the emission lifetime to be increased in the presence of the co-dopants. Figure 6 shows the $^4I_{9/2}$ emission lifetimes as a function of various Er^{3+} concentrations as well as co-doping with Gd^{3+} or Na^+ ions. Unlike in RE-doped CaF_2, Er^{3+}:BaF_2 does not appear to undergo significant nonradiative relaxation due to clustering, and Er^{3+} emission does not appear to be affected by co-doping with Gd^{3+} or Na^+.

Table 3 The investigated Er^{3+}:BaF_2 crystals via co-doping with various concentrations of non-optically active ion Gd^{3+} as well as co-doping with a charge-compensating ion Na^+. The singly doped Er^{3+}:BaF_2 crystals with different concentrations are also listed.

Singly doped Er^{3+}	Co-doped Na^+	Co-doped Gd^{3+}
1% Er	1% Er, 1% Na	1% Er, 3% Gd
2% Er	2% Er, 2% Na	3% Er, 6% Gd
3% Er	3%Er, 3% Na	6% Er, 6% Gd
4% Er	6% Er, 6% Na	…
6% Er	10% Er, 10% Na	…
8% Er	…	…
10% Er	…	…

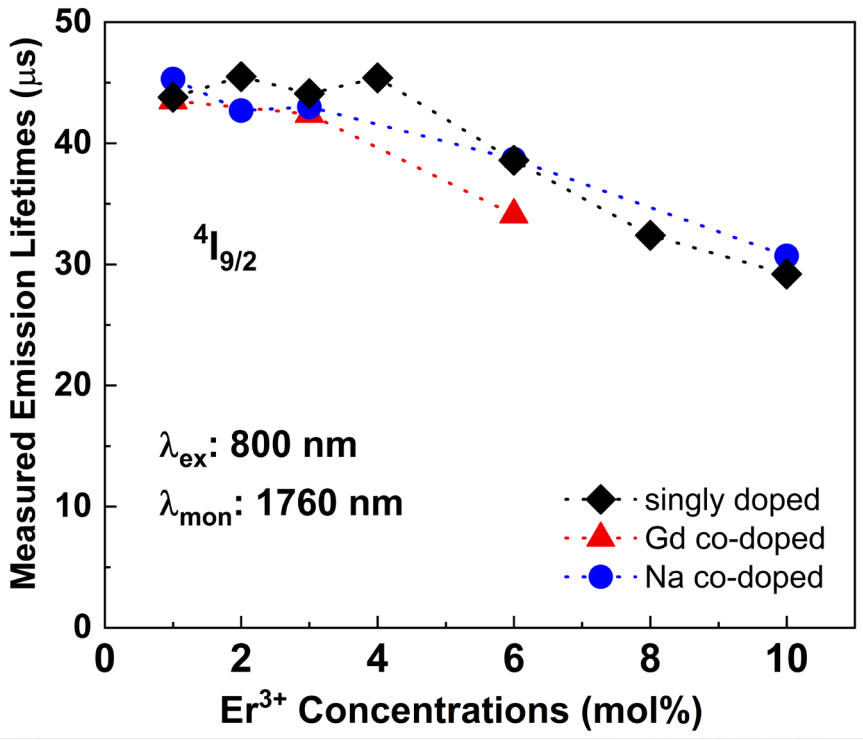

Fig. 6 Measured lifetimes as a function of Er^{3+} concentration as well as co-doping with a buffer ion Gd^{3+} and charge-compensation Na^+ ions at room temperature

4. Conclusions

Preliminary results of spectroscopic evaluation of Er^{3+}-doped BaF_2 crystals, grown by the Bridgman technique, were investigated. The absorption spectrum of Er^{3+}:BaF_2 displayed the characteristic Er^{3+} transitions in the visible and IR spectral region. Optical pumping into the $^4I_{15/2} \rightarrow {}^4I_{9/2}$ absorption band at approximately 800 nm (chosen to simulate diode pumping) resulted in the observation of several mid-IR Er^{3+} fluorescence bands, which correspond to the $^4I_{11/2} \rightarrow {}^4I_{13/2}$ (~2.74 μm), $^4F_{9/2} \rightarrow {}^4I_{9/2}$ (~3.5 μm), and $^4I_{9/2} \rightarrow {}^4I_{11/2}$ (~4.48 μm) transitions. The room temperature fluorescence lifetimes of the first four excited states of Er^{3+}:BaF_2 were determined to be approximately 16 ms ($^4I_{13/2}$), 9.4 ms ($^4I_{11/2}$), 0.047 ms ($^4I_{9/2}$), and 0.396 ms ($^4F_{9/2}$). An analysis of the temperature dependence of the 4.48-μm emission lifetime revealed that the $^4I_{9/2}$ state exhibited some contribution of multiphonon relaxation, and it can be speculated that nonradiative decay through multiphonon relaxation might not be the only process active in the Er^{3+}:BaF_2 crystal. The large difference between measured low-temperature lifetime and calculated radiative lifetime (Judd–Ofelt analysis) indicates nonradiative decay through other processes, such as energy transfer between RE ions or other impurities in the crystal. The mid-IR emission cross section at 4.48 μm was determined to be approximately 0.14×10^{-20} cm^2. The obtained spectroscopic parameters for 4.48-μm emission compare favorably with other Er^{3+}-doped materials, which underline the potential of this material for mid-IR laser applications. Initial laser experiments for mid-IR emissions at 4.48 μm are in progress at room and liquid nitrogen temperatures.

5. References

1. Velazquez M, Ferrier A, Doualan JL, Moncorge R. Rare-earth doped low phonon energy halide crystals for mid-infrared sources. In: Al-Khursan A, editor. Solid-State Laser. London (UK): IntechOpen; 2012. pp. 119–142.

2. Eichhorn M. Quasi-three-level solid-state lasers in the near and mid infrared based on trivalent rare earth ions. Appl Phys B. 2008;93:269–316.

3. Bowman SR, Searles SK, Jenkins NW, Qadri SB, Skelton EF, Ganem J. Diode pumped room temperature mid-infrared erbium laser. In: Marshall C, editor. Advanced Solid-State Lasers. Washington (DC): Optical Society of America; 2001. pp. 154–156. OSA trends in optics and photonics, Vol. 50.

4. Orlovskii YV, Basiev TT, Pukhov KK, Glushkov NA, Alimov OK. Multiphonon relaxation of mid-IR transitions of RE ions in fluorite type crystals. In: Quarles G, editor. Advanced Solid-State Photonics (TOPS) 2004. Washington (DC): Optical Society of America; 2004. Paper 440. OSA trends in optics and photonics, Vol. 94.

5. Brown E, Fleischman Z, Merkle LD, Rowe E, Burger A, Payne SA, Dubinskiy M. Optical spectroscopy of holmium doped K_2LaCl_5. J Lumin. 2018;196:221–226.

6. Bitam A, Khiari S, Diaf M, Boubekri H, Boulma E, Bensalem C, Guerbous L, Jouart JP. Spectroscopic investigation of Er^{3+} doped BaF_2 single crystal. Opt Mater. 2018;82:104–109.

7. Labbe C, Doualan JL, Camy P, Moncorge R, Thuau M. The 2.8 μm laser properties of Er^{3+} doped CaF_2 crystals. Opt Comm. 2002;209:193–199.

8. Svejkar R, Sulc J, Jelinkova H, Kubecek V, Ma W, Jiang D, Wu Q, Su L. Diode-pumped Er:SrF_2 laser tunable at 2.7 μm. Opt Mater Exp. 2018;8:1025–1030.

9. Orlovskii YuV, Basiev TT, Pukhov KK, Alimov OK, Glushkov NA, Konyushkin VA. Low-phonon BaF_2:Ho^{3+}, Tm^{3+} doped crystals for 3.5–4 μm lasing. Opt Mater. 2010;32:599–611.

10. Soulard R, Moncorge R, Cai Z, Doualan JL, Xu H, Braud A, Camy P. Spectroscopic properties of Er-doped fluoride crystals and glasses for 3.5 μm laser operation. In: OSA Laser Congress (ASSL, LAC); 2017 Oct 1–5; Nagoya, Aichi, Japan. Washington (DC): Optical Society of America; 2017. Paper JTu2A.5.

11. Gomes L, Librantz A, Jagosich F, Alves W, Ranieri I, Baldochi S. Energy transfer rates and population inversion of $^4I_{11/2}$ excited state of Er^{3+} investigated by means of numerical solutions of the rate equations system in Er:$LiYF_4$ crystal. J Appl Phys. 2009;106:10350 (1–9).

12. Labbe C, Doualan JL, Moncorgé R, Braud A, Camy P. Excited-state absorption and fluorescence dynamics of Er^{3+}:KY_3F_{10}. Opt Mater. 2018;79:279–288.

13. Labbe C, Doualan JL, Moncorgé R, Braud A, Camy P. Excited-state absorption and fluorescence dynamics in Er:CaF_2. J Lumin. 2018;200:74–80.

14. Kaminskii AA. Crystalline lasers: physical processes and operating schemes. Boca Raton (FL): CRC Press; 1996.

15. Aull BF, Jenssen HP. Vibronic interactions in Nd:YAG resulting in nonreciprocity of absorption and stimulated emission cross sections. IEEE Quantum Electron. 1982;18:925–930.

List of Symbols, Abbreviations, and Acronyms

ICP-OES	inductively coupled plasma optical emission spectroscopy
IR	infrared
NIR	near infrared
RE	rare earth
UV	ultraviolet

1 (PDF)	DEFENSE TECHNICAL INFORMATION CTR DTIC OCA
1 (PDF)	CCDC ARL FCDD RLD DCI TECH LIB
4 (PDF)	CCDC ARL FCDD RLS RL EE BROWN M DUBINSKIY Z FLEISCHMAN J MCKAY